

BENCHMARK OF STRONG-STRONG BEAM-BEAM SIMULATION OF THE KINK INSTABILITY IN AN ELECTRON ION COLLIDER DESIGN*

J. Qiang[#], R. D. Ryne, LBNL, Berkeley, CA94720, U.S.A.

Y. Hao, BNL, Upton, Long Island, NY 11973, U.S.A.

Abstract

The kink instability limits the performance of a potential linac-ring based electron-ion collider design. In this paper, we report on the simulation study of the kink instability using a self-consistent strong-strong beam-beam model and benchmark these results with a strong-weak model and an analytical model.

INTRODUCTION

An electron-ion collider (EIC) as the highest priority from the Nuclear Physics Office long range plan recommendation has been actively studied at both BNL and Jlab. The linac-ring collider is an important option for the EIC design due to the fact that it can produce higher luminosity than the ring-ring based collider [1]. However, the beam-beam effect between the electron beam and the proton/ion beam significantly limits the final collider performance. Besides causing the electron beam mismatch at the interaction point and transverse phase space distortion, it also causes the proton/ion beam unstable and emittance blow up through the so-called kink instability [2-3]. Here, the kink instability is similar to the conventional wakefield head-tail instability except that the wakefield in the kink instability is from the electron beam-beam force excited by the small offset of the proton beam. Such an instability limits final luminosity of the linac-ring collider.

COMPUTATIONAL SETUP

All self-consistent simulations presented in this study were done using a strong-strong collision model implemented in the code BeamBeam3D [4]. The BeamBeam3D is a parallel three-dimensional particle-in-cell code to model beam-beam effect in high-energy colliders. This code includes a self-consistent calculation of the electromagnetic forces (beam-beam forces) from two colliding beams (i.e. strong-strong modeling), a linear transfer map model for beam transport between collision points, a stochastic map to treat radiation damping, quantum excitation, an arbitrary orbit separation model, and a single one-turn map to account for chromaticity effects. Here, the beam-beam forces are calculated by solving the Poisson equation using an FFT-based algorithm. The longitudinal bunch length effect is included using multiple slices during the beam-beam interaction. This makes it suitable to study the kink instability, which depends on the bunch length of the colliding beams. It can also handle multiple bunch collisions at multiple interaction points (IPs), and various

beam-beam compensation schemes. The parallel implementation is done using a particle-field decomposition method to achieve a good load balance. It has been applied to studies of the beam-beam effect at a number of high energy colliders such as RHIC, Tevatron, LHC, and KEK-B [5-8].

The parameters used in this study are given in the following table. Here, the electron bunch length is much shorter than the proton bunch length. It collides once with the proton beam, and a new electron beam is generated from the linac at the interaction point every turn while the proton beam circulating around one of the RHIC rings following a one-turn transfer map and comes back to collide with the electron beam again and again. As the electron bunch length is much shorter than the proton bunch, it undergoes the proton bunch subject to the strong beam-beam forces from the proton beam. Before carrying out detailed physics study, we checked the convergence of relevant physics with respect to the choice of the numerical parameters, especially the number of longitudinal slices for each beam. Figure 1 shows the electron beam emittances after one collision as a function of the number of slices for the proton beam using 4 and 8 slices for the electron beam. It is appears that 4 slices for the electron beam will be sufficient while 160 slices are needed for the proton beam. The macroparticle for each beam used in the simulation is about 1 million.

Table 1: Physical Parameters Used in the Simulations

Parameter	E	P
$N(10^{11})$	0.07	3
ε_n [μm]	23	0.2
β^* [cm]	5	5
Q_x		0.685
Q_y		0.675
Q_z		0.004
bunch length [cm]	0.4	5
Energy [GeV]	15.9	250
beam-beam param.	2.9	0.004

*Work supported by the Director of the Office of Science of the US Department of Energy under Contract no. DEAC02-05CH11231 and by the FP7 HiLumi LHC <http://hilumilhc.web.cern.ch>

[#]jqliang@lbl.gov

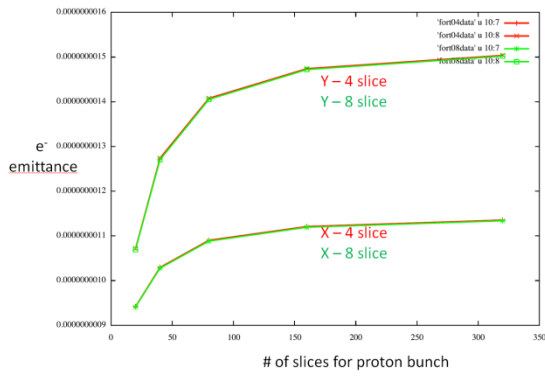


Figure 1: Electron beam emittances after a collision with the proton beam as a function of the number of slices used for proton bunch in the simulation with four (red) and eight (green) slices for the electron bunch.

SIMULATION RESULTS

We first check the electron beam evolution during the collision with the proton beam. Due to the opposite charge of two colliding beams, the electron beam inside the proton beam will be focused by the beam-beam force from the proton beam. This effect is also called the pinch effect. Figure 2 shows the electron beam transverse rms effective emittance (half of the average value of Courant-Snyder invariant of all macroparticles) and rms geometric emittance as a function slice number across the proton beam. The bottom plot is from the self-consistent strong strong simulation while the top plot is from a two pass weak-strong model, EPIC [9]. It is seen that both models agree with each other quite well. The electron undergoes betatron oscillation inside the proton beam and the transverse emittance oscillates inside the proton beam. The rms geometry emittance after collision increases by about 50% while the effective emittance growth increases by more than 100%. This large effective emittance growth is due the mismatch caused by the linear beam-beam forces. Figure 3 shows the electron beam transverse phase space after the colliding with the proton beam. The bottom plot is from the self-consistent simulation while the top plot is from the two pass weak-strong simulation. A large tail is seen in the electron beam transverse phase space after the collision from both models. This large tail is due to the strong nonlinear beam-beam force from the proton beam. Such a large amplitude tail should be carefully handled in order to avoid particle losses after the collision, in the process of energy recovery through several recirculation passes.

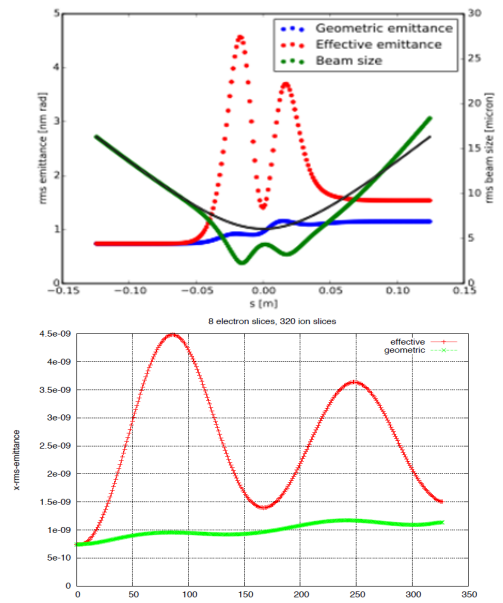


Figure 2: Electron beam rms effective emittance and geometric emittance as a function longitudinal positions. The top plot is from the EPIC simulation, and the bottom plot is from the BeamBeam3D simulation.

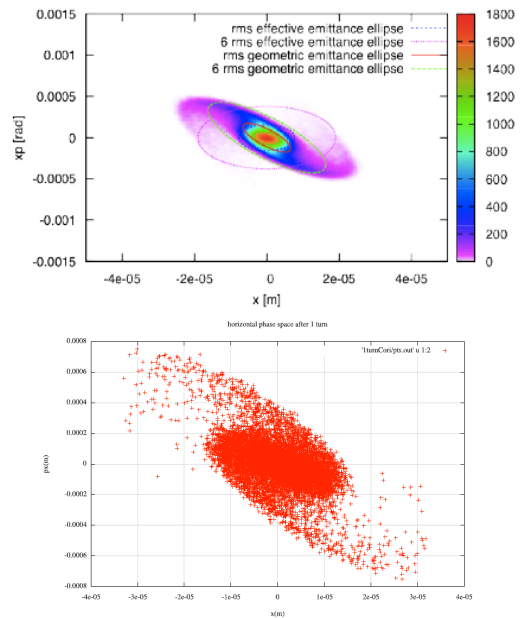


Figure 3: Electron beam transverse phase space after collision from the EPIC simulation and from the BeamBeam3D simulation (bottom).

The kink instability is caused by the collective motion of electron beam inside the ion beam. A small imperfection from the head of the ion beam will be amplified and pass through the rest of the beam in the instability. The threshold of the instability can be analytically calculated using a 2-particle model or a multi-particle model [3]. Figure 4 shows the threshold of the kink instability as a function electron disruption parameter from the 2-particle model (red), the multi-particle model (blue), and four strong-strong simulations (purple)

diamond). Here, two simulations are in the unstable regime while the other two are in the stable regime. Figure 5 shows the emittance evolution of the proton beam from these four simulations. It is seen that when electron disruption parameter increases and moves into the unstable regime, significant emittance growth is observed. Outside the unstable regime, the proton beam shows little emittance growth.

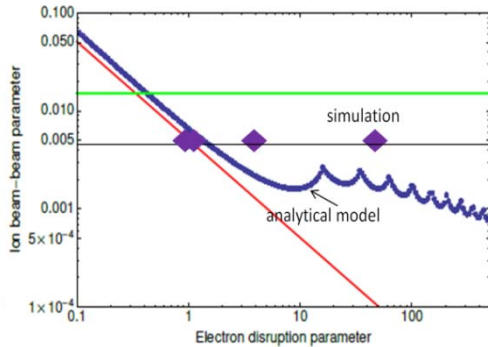


Figure 4: The threshold of kink instability as a function electron disruption parameter from the 2-particle model (red), the multi-particle model (blue), and simulations (purple diamond).

It is well known that the head tail instability can be damped by the Landau damping with machine chromaticity. Figure 6 shows the proton beam emittance

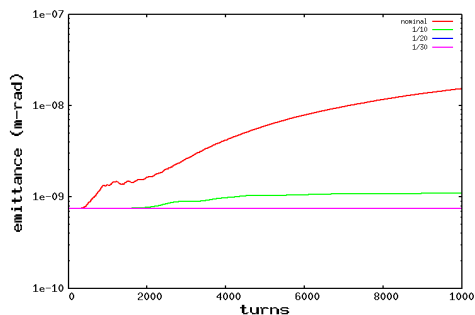


Figure 5: The proton beam emittance evolution with four electron disruption parameters.

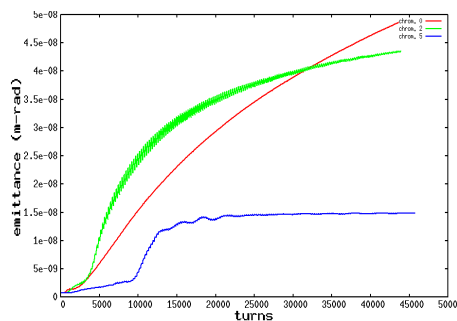


Figure 6: The proton beam emittance evolution with different chromaticities.

evolution with three machine linear chromaticities (0, 2, and 5). It is seen that with the increase of the chromaticity, the maximum growth of the proton beam decreases. However, using only the chromaticity is not sufficient to suppress the kink instability (without using

too large chromaticity). A feedback system is needed to effectively suppress this instability. Figure 7 shows the proton beam emittance evolution with different bandwidth. It is seen that the feedback system should have a sufficient large bandwidth (≥ 500 MHz) in order to suppress the instability. Figure 8 shows the proton beam emittance evolution with different feedback gains. The gain factor greater than 0.05 is needed in order to suppress the instability in the current design.

CONCLUSIONS

In summary, in this paper, we studied the kink instability using a self-consistent strong-strong beam-beam simulation model. The electron beam emittance and transverse phase space after the collision from the strong-strong simulation and from the strong-weak model agrees with each other quite good. The strong-strong simulation results also agree well with the analytical model about the instability threshold. Using the strong-strong simulation, we also checked the effects from the machine chromaticity and found that the modest machine chromaticity is not sufficient to suppress the instability. A feedback system with appropriate bandwidth and gain is needed in order to suppress the kink instability for the current linac-ring design.

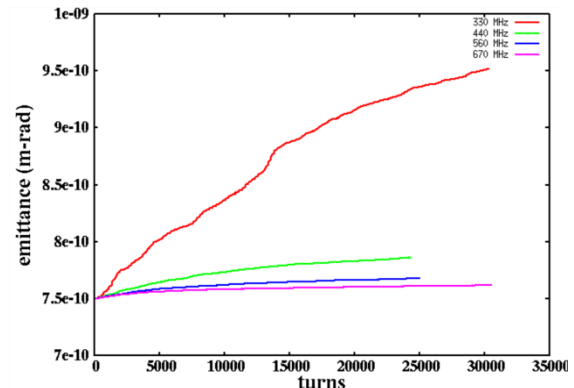


Figure 7: The proton beam emittance evolution with different feedback bandwidths.

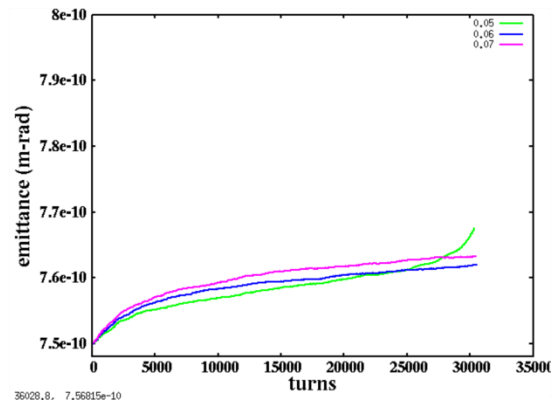


Figure 8: The proton beam emittance evolution with different feedback gains.

REFERENCES

- [1] V. Ptitsyn *et al.*, Technical Report, C-AD, BNL, 2007.
- [2] Y. Hao and V. Ptitsyn, *Phys. Rev. ST Accel. Beams*, vol. 13, 071003, 2010.
- [3] Y. Hao, V. N. Litvinenko, and V. Ptitsyn, *Phys. Rev. ST Accel. Beams*, vol. 16, p. 101001, 2013.
- [4] J. Qiang *et al.*, *J. of Comp. Phys.*, vol. 198, p. 278, 2004.
- [5] J. Qiang *et al.*, *Nucl. Instr. & Meth. in Phys. Res.* vol. A558, p. 351, 2006.
- [6] J. Qiang *et al.*, in *Proc. of IPAC 2015*, p. 2210.
- [7] J. Qiang *et al.*, *Proc. HALO'03*, May 19-23, Montauk, NY, 2003, p. 278.
- [8] J. Qiang *et al.*, *Proc. of Particle Accelerator Conf. 2003*, Portland, Oregon, May 12-16, p. 3401.
- [9] Y. Hao, Ph.D. thesis, Indiana University, 2008.